CrystEngComm

Accepted Manuscript

This article can be cited before page numbers have been issued, to do this please use: D. Markad and S. Mandal, *CrystEngComm*, 2017, DOI: 10.1039/C7CE01666B.

ROYAL SOCIETY OF CHEMISTRY

rsc.li/crystengcomm

View Article Online
DOI: 10.1039/C7CE01666B

Journal Name

RSCPublishing

ARTICLE

An exploration into the amide-pseudo amide hydrogen bonding synthon between a new coformer with two primary amide groups and theophylline†

Cite this: DOI: 10.1039/x0xx00000x

Received xxxxxxxxx
Accepted xxxxxxxxx

DOI: 10.1039/x0xx00000x

www.rsc.org/

Datta Markad[a] and Sanjay K. Mandal[a]*

A cocrystal between a new coformer with two primary amide groups, 2,2'-((1,4-phenylenebis(methylene))-bis((pyridin-2-ylmethyl)azanediyl))diacetamide (**2-BPXG**) and Theophylline (**THP**) was selected as a model system to (a) demonstrate the presence of the rare amide-pseudo amide hydrogen bonding motif in it and identify further structural features by single crystal X-ray diffraction, and (b) establish its relevant physicochemical properties through a comparison with the coformer by Fourier-transform infrared (FT-IR) spectroscopy, differential scanning calorimetry (DSC), thermogravimetric analysis (TGA), differential thermal analysis (DTA), powder X-ray diffraction (PXRD), and hot stage microscopy (HSM). To the best of our knowledge, this is the first example where a coformer with two primary amide groups has been used to form the amide-pseudo amide hydrogen bonding motif. The co-crystal (**2-BPXG·4THP**) crystallizes in the triclinic space group *P*-1 with Z = 1 where the unit cell contains one **2-BPXG** molecule and four **THP** molecules. Whereas, the coformer **2-BPXG** crystallizes in the monoclinic space group $P2_1/c$ with Z = 2 (the asymmetric unit contains half of the molecule). Surprisingly, only **2-BPXG** (compared to other coformers with aliphatic spacers between the two alkyl nitrogen atoms), which does not form the amide-amide hydrogen bonding motif within itself, paves the way to form the amide-pseudo amide hydrogen bonding motif $R_2^2(9)$ with **THP**. An overall 2D supramolecular network is formed in **2-BPXG** through the interlinking of the ladder-shaped layers (which are generated through strong hydrogen bonding between one of the N-H bonds and pyridine nitrogen) *via* strong hydrogen bonding between the other N-H bond and the carbonyl group of an adjacent molecule. On the other hand, the coformer with one primary amide group on each end generates a ladder-shaped layer in the cocrystal through hydrogen bonding interactions with **THP** molecules. These ladder-shaped layers are further connected *via* strong π-π (centroid to centroid distance: 3.68 Å) and weak C-H···O interactions between the **THP** molecules to form an overall 3D supramolecular network in the cocrystal. Hydrogen bond propensities, Hirshfeld surface analysis and quantitative crystal structure analysis of both coformer and cocrystal allowed us to understand the amide-pseudo amide hydrogen bonding motif in detail.

Introduction

Crystal engineering plays an important role in the preparation of multicomponent crystals with enhanced physicochemical properties.[1-4] Pharmaceutical co-crystallization has been a center stage of late due to its capability of enhancing the proficiency of the active pharmaceutical ingredient (API). In this developing field, much consideration has been provided to the search of new cocrystals, while the properties of the solid phases in such systems as well as the possibility of industrial scale production are still immature ranges.[5-9] As a first step for the co-crystallization of an API, one needs to consider the functional groups that are present in it for the selection of coformers with complementary functionalities based on expected moderate to strong hydrogen bonding and/or π-π interactions.[10] On the other hand, for the bioavailability of an API co-crystal, the pharmaceutical/regulatory acceptability of the coformer has to be considered. Thus, the stduy of a new coformer for cocrystal formation with an API requires proper toxicity evaluation. However, in the absence of such toxicity data one can pursue such cocrystallization study with a focus on structural/supramolecular aspects, which can be translated to other biocompatible compounds with similar moities to provide an impetus without the expensive toxicity evaluation initially. This work was carried out with such a goal by designing a new coformer with two primary amide groups, the first example in this field. If

View Article Online
DOI: 10.1039/C7CE01666B
Journal Name

desired, we may consider its toxicity evaluation for future research work showing its usability in pharmaceuticals and can be fortunate to see that it is biocompatible due to its simple structure.

There are various tools available for the prediction of cocrystal formation, the *in silico* method and hydrogen bond propensity calculations being the commonly used ones. The former method takes into consideration of the structural and energetic factors, while the latter involves calculations based on the CSD statistical database.[11-14] Here, we have chosen the hydrogen bond propensity tool, which evaluates earlier reported crystal structures available in the CSD database, where the likelihood can be used to foresee whether two molecules will co-crystallize or not.

For components with an amide or a pseudo amide functionality, three types of synthons shown in Scheme 1 can occur in their cocrystals: amide-amide homosynthon with a graph set notation $R_2^2(8)$, amide-pseudo amide heterosynthon with a graph set notation $R_2^2(9)$ and pseudo amide-pseudo amide homosynthon with a graph set notation $R_2^2(10)$; the symbolism[15] indicates that the motif takes the form of a hydrogen-bonded ring consisting of 8 or 9 or 10 atoms in total, 2 of which act as hydrogen-bond donors and 2 of which act as hydrogen-bond acceptors. Thus, the two homosynthons are in competition with the heterosynthon for such a scenario. While the amide-amide synthon has been widely known in supramolecular chemistry,[6] the amide-pseudo amide synthon is not so common. An API with a pseudo amide functionality is **THP** (see Scheme 2 for its structure), which provides several pharmaceuticals utilized as bronchodilators that unwind the muscles in the breathing tubes like asthma and chronic obstructive pulmonary disease (COPD). In **THP**, the imidazole NH and =CH group act as hydrogen-bond donors and the imidazole nitrogen and the two carbonyl oxygen atoms act as hydrogen-bond acceptors. The presence of both hydrogen bond donors and acceptors in **THP** adds an extra element of complexity in considering the design of its hydrogen-bonded cocrystals. On the other hand, **THP** is known to exist in seven polymorphic forms.[16-23] Out of three anhydrous forms, Form II has been considered as the most stable form at room temperature.[24] Reversible formation of the Form II to its hydrate form is an undesired feature that must be taken into account in the formulation procedure. For this reason, the dissociation of cocrystals upon exposure to humidity is an important factor. In this regard, the work by Jones and coworkers on Caffeine with various dicarboxylic acids for a remedy provides an excellent example.[25] Among the efforts towards overcoming this problem, the most important one is the prevention of the formation of the hydrate form by the preparation of cocrystals, which has involved so far a high number of coformers. Only three of them had coformers with an amide functionality that provided the first examples of the amide-pseudo amide motif for the APIs reported in the literature between 1986-2008.[26-27] Furthermore, only recently Eddleston *et al*. investigated an amide-pseudo amide hydrogen bonding motif within a series of coformers with one primary amide group and **THP** cocrystals.[28] Thus, the study of such motif with new examples is highly desired.

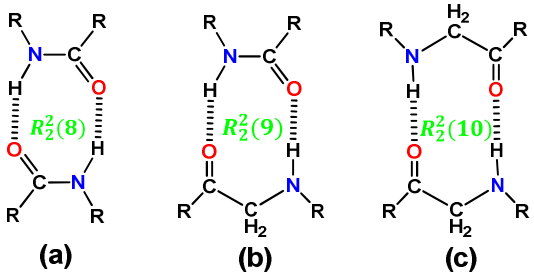

Scheme 1 Schematic representation of (a) amide-amide, (b) amide-pseudo amide, and (c) pseudo amide – pseudo amide synthons with the graph set notations.

Based on the properties described above for **THP**, we designed a new coformer with two primary amide groups, namely 2,2'-((1,4-phenylenebis(methylene))bis((pyridin-2-ylmethyl)azanediyl))diacetamide (**2-BPXG**), shown in Scheme 2 to explore and identify structural features and relevant physicochemical properties of its cocrystal with Form II of **THP**. The coformer has several special features, such as two primary amide groups ($-CONH_2$) acting either as a hydrogen bond acceptor (=O) or a hydrogen bond donor ($-NH_2$) along with the pyridine nitrogens also acting as hydrogen bond acceptors. Therefore, it is a suitable molecular entity for forming a cocrystal with **THP** which possesses complementary functionalities mentioned above.

Herein, we report the synthesis, structural characterization and physicochemical properties of **2-BPXG** and its cocrystal, **2-BPXG·4THP**, with the help of a number of number of analytical techniques, such as single crystal X-ray diffraction (SCXRD), Fourier-transform infrared (FT-IR) spectroscopy, differential scanning calorimetry (DSC), thermogravimetric analysis (TGA), differential thermal analysis (DTA), powder X-ray diffraction (PXRD), and hot stage microscopy (HSM). To the best of our knowledge, this is the first example where a coformer with two primary amide groups has been used to form the amide-pseudo amide hydrogen bonding motif.

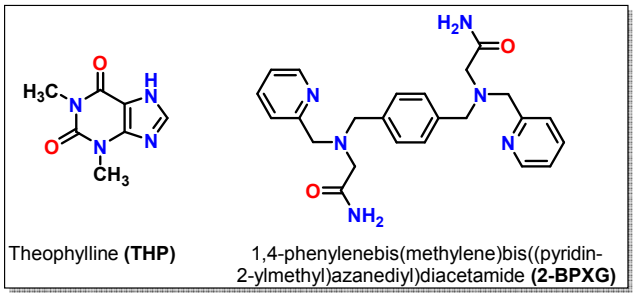

Scheme 2 Structures of **THP** and **2-BPXG**.

Experimental section

Materials and methods. All chemicals and solvents used for synthesis were obtained from commercial sources and were used as received, without further purification. All reactions were carried out under aerobic conditions.

Journal Name View Article Online DOI: 10.1039/C7CE01666B ARTICLE

Hydrogen bond propensity calculations were performed using the Solid Form module available as part of Mercury v3.5.1 software from the Cambridge Crystallographic Data Centre (CCDC) with version 5.35 of the Cambridge Structural Database. The default options were used throughout (including functional group selection).

Physical measurements. The ^{1}H NMR spectrum of **2-BPXG** was obtained in $CDCl_3$ solution at 25 °C on a BrukerARX-400 spectrometer; chemical shifts are reported relative to the residual solvent signals. Melting points were determined by a Büchi M-565 instrument. TGA and DTA were carried out from 25 to 330 °C (at a heating rate of 10 °C/min) under dinitrogen atmosphere on a Shimadzu DTG-60. DSC measurements were performed on a Perkin Elmer DSC 8000 with a scan rate of 10 °C/min. IR spectra were measured in the 4000-400 cm^{-1} range on a Perkin-Elmer Spectrum I spectrometer with samples prepared as KBr pellets. Hot stage microscopy experiments were performed on a ZEISS Discovery V12 microscope using a LIKAM hot stage controlled by the Linksys32 software. Contact thermal microscopy was conducted by heating from room temperature at a 10 °C/min heating rate and was discontinued once all the material had melted.

Synthesis of 2,2'-((1,4-phenylenebis(methylene))bis((pyridin-2-ylmethyl)azanediyl))diacetamide (2-BPXG). It is prepared in two steps where N,N'-(1,4-phenylenebis (me-thylene))bis(1-(pyridin-2-yl)methanamine), **2-BPXD**, is an intermediate. **Step 1: Synthesis of 2-BPXD.** In a 50 mL round-bottom flask (RBF), a solution of 1,4-phenylenedimethanamine (500 mg, 3.6 mmol) in 5 mL methanol was added with picolinaldehyde (0.7 mL, 7.3 mmol) in a drop wise manner at room temperature. Within half an hour a white slurry was formed and the resulting slurry was stirred for another 5 h. An excess of sodium borohydride (420 mg, 1.5 equiv) was added slowly to the above solution at 0 °C and stirred for 6 h. The resulting light yellow oily product was isolated from the reaction mixture by extracting with chloroform followed by drying with anhydrous $MgSO_4$ and removal of solvent under vacuum. Yield: 1.1 g (94%). ^{1}H NMR (400 MHz, $CDCl_3$, δ ppm): 8.55(2H, d), 7.63(2H, t), 7.31(4H, s), 7.29(2H, d), 7.17(2H, m), 3.91(4H, s), 3.82(4H, s), 2.15(2H, s). ^{13}C NMR (100 MHz, $CDCl_3$, δ ppm): 159.43, 149.08, 138.58, 136.26, 128.15, 122.20, 121.76, 54.21, 52.99. Selected FTIR peaks (KBr cm^{-1}): 3306 (br, N-H stretch), 2928(m, aromatic C-H stretch), 2855 (m), 1592 (s, pyridine C=C stretch), 1570 (s, pyridine C=N stretch), 1471 (m), 1434 (m), 1300 (m, aliphatic C-H stretch), 1118 (m, aliphatic C-C stretch), 1048 (s), 996 (s), 760 (s), 631 (m).

Step 2: To a solution of **2-BPXD** (320 mg, 1 mmol), obtained from the step 1 above, in 10 mL dry acetonitrile taken in a 50 mL RBF under N_2 atmosphere, K_2CO_3 (2.78 g, 20 mmol) was added through a funnel at once and allowed to stir for 30 minutes. A solution of 2-bromoacetamide (278 mg, 2 mmol) in dry acetonitrile (15 mL) was added dropwise to the above mixture. The mixture was heated under reflux for 5 h and allowed to cool down to room temperature, filtered using G-4 crucible; the residue obtained was thoroughly washed with methanol (10 mL X 2). The filtrate obtained was evaporated to dryness followed by extraction of the product with dry methanol and filtration to remove excess K_2CO_3 and KBr (by-product). Upon removal of methanol under vacuum from the filtrate, the resultant oily substance was cooled to 0 °C and treated with 10 mL $CHCl_3$. Further filtration and evaporation of the solvent provided the desired product as a light yellow solid. Yield: 348 mg (80%). ^{1}H NMR (400 MHz, $CDCl_3$, δ ppm): 8.59(2H, d), 7.98(2H, t), 7.67(2H, m), 7.24(2H, d), 7.21(4H, s), 3.81(4H, s), 3.64(4H, s), 3.18(4H, s). ^{13}C NMR (100 MHz, $CDCl_3$, δ ppm): 174.34, 157.99, 149.39, 136.85, 136.44, 128.97, 122.99, 122.32, 60.64, 58.80, 57.34. Selected FTIR peaks (KBr cm^{-1}): 3409(s), 2854(m), 1656 (s, amide C=O stretch), 1593(s, pyridine C=C stretch), 1476 (s, pyridine C=N stretch), 143(m), 1399(m, aliphatic C-H stretch), 1255(s, aliphatic C-C stretch), 1128(s), 987(s), 772(s), 619(m). M.P.: 164-166 °C. MS (ESI-TOF): m/z calcd for [(**2-BPXG**)H]$^+$, 433.2300; found, 433.2307.

The ^{1}H and ^{13}C NMR spectra of **2-BPXD** and **2-BPXG** are shown in Fig. S1-S4, respectively (ESI).

Synthesis of 2-BPXG·4THP. 10 mg (0.023 mmol) of **2-BPXG** and 16.6 mg (0.092 mmol) of **THP** were dissolved in 6 mL ethanol. The mixture was heated to 60 °C to make a clear solution (due to moderate solubility of 2-BPXG in ethanol) and stirred for 4 hours at that temperature. Crystals were obtained via slow evaporation under ambient conditions after 2 days. Yield: 23 mg (87%). Selected FTIR peaks (KBr, cm^{-1}): 3424 (s), 3270 (w), 3114 (w), 3056 (w), 2984 (w), 2820 (w), 2614 (w), 1704 (s), 1648 (s), 1562 (s), 1434 (s), 1242 (s), 1174 (s), 984 (s), 926 (s), 764 (s), 612 (s), 500 (s). M.P.: 234-236 °C.

Single Crystal X-ray structure analysis. Following the general procedures published earlier,[29] from a batch of crystals of each compound a single crystal was placed inside a nylon loop on a goniometer head which was then attached to the instrument. Initial crystal evaluation and data collection were performed on a Kappa APEX II diffractometer equipped with a CCD detector (with the crystal-to-detector distance fixed at 60 mm) and sealed-tube monochromated MoKα radiation and interfaced to a PC that controlled the crystal centering, unit cell determination, refinement of the cell parameters and data collection through the program APEX2.[30] By using the program SAINT[30] for the integration of the data, reflection profiles were fitted, and values of F^2 and $\sigma(F^2)$ for each reflection were obtained. Data were also corrected for Lorentz and polarization effects. The subroutine XPREP[30] was used for the processing of data that included determination of space group, application of an absorption correction (SADABS),[30] merging of data, and generation of files necessary for solution and refinement. The crystal structures were solved and refined using SHELX 97.[31] In each case, the space group was chosen based on systematic absences and confirmed by the successful refinement of the structure. Positions of most of the non-hydrogen atoms were obtained from a direct methods solution. Several full-matrix

View Article Online
DOI: 10.1039/C7CE01666B Journal Name

least-squares/difference Fourier cycles were performed, locating the remainder of the non-hydrogen atoms. In the final difference Fourier map in each case there was no other significant peaks >1 e/Å^3. All non-hydrogen atoms were refined with anisotropic displacement parameters. All hydrogen atoms were placed in ideal positions and refined as riding atoms with individual isotropic displacement parameters. Crystallographic parameters and basic information pertaining to data collection and structure refinement for all compounds are summarized in Table 1. All figures were drawn using Mercury v3.5.1[32] and hydrogen bonding parameters were generated using PLATON.[33] The final positional and thermal parameters of the non-hydrogen atoms for all structures are listed in the CIF files (ESI).

Powder X-ray studies. Data were recorded on a Rigaku Ultima IV diffractometer equipped with a 3 kW sealed tube Cu Kα X-ray radiation (generator power settings: 40 kV and 40 mA) and a DTex Ultra detector using BB geometry (2.5° primary and secondary solar slits, 0.5° divergence slit with 10 mm height limit slit). Each sample was ground into a fine powder using a mortar and a pestle and was placed on a glass sample holder that was placed on the sample rotation stage (120 rpm) attachment. The data were collected over an angle range 5° to 50° with a scanning speed of 1° per minute with 0.01° steps.

Table 1 Crystal Structure Data and Refinement Parameters for **2-BPXG** and **2-BPXG·4THP.**

Compound	**2-BPXG**	**2-BPXG·4THP**
Chemical formula	$C_{24}H_{28}N_6O_2$	$C_{24}H_{28}N_6O_2$, $4(C_7H_8N_4O_2)$
Formula Weight (g/mol)	432.52	1153.22
Temperature (K)	298(2)	296(2)
Wavelength (Å)	0.71073	0.71073
Crystal system	Monoclinic	Triclinic
Space group	$P2_1/c$	*P-1*
a (Å)	14.5865(9)	9.536(16)
b (Å)	8.2327(4)	11.74(2)
c (Å)	10.1220(5)	12.81(2)
α (°)	90	96.84(2)
β (°)	94.055(2)	93.49(2)
γ (°)	90	94.57(2)
Z	2	1
Volume (Å^3)	1212.47(11)	1416(4)
Density (g/cm^3)	1.185	1.352
μ (mm^{-1})	0.079	0.098
Theta range (°)	1.40 to 25.00	1.61 to 25.00
F(000)	460	606
Reflections Collected	7228	15263
Independent reflections	2119	4851
Reflections with I >2σ(I)	1453	2814
R_{int}	0.0436	0.0487
Number of parameters	145	383
GOF on F^2	1.050	1.089
Final R_1[a]/wR_2[b] (I > 2σ(I))	0.0469/0.1356	0.0558/0.1535
R_1[a]/wR_2[b] (all data)	0.0716/0.1522	0.0941/0.1861
Largest diff. peak and hole	0.130 and -0.141	0.240 and -0.239

[a]$R_1 = \Sigma||Fo| - |Fc||/\Sigma|Fo|$. [b]$wR_2 = [\Sigma w(Fo^2 - Fc^2)^2/\Sigma w(Fo^2)^2]^{1/2}$, where $w = 1/[\sigma^2(Fo^2) + (aP)^2 + bP]$, $P = (Fo^2 + 2Fc^2)/3$.

Results and discussion

Crystal growth

2-BPXG. Rectangular-shaped crystals suitable for single crystal X-ray study were obtained by dissolving 10 mg of **2-BPXG** in

Journal Name
View Article Online
DOI: 10.1039/C7CE01666B ARTICLE

4 mL acetonitrile and keeping the solution for slow evaporation at room temperature for 5 days.

2-BPXG·4THP. Needle-shaped crystals were obtained in almost quantitative yield as described in the experimental section.

Based on the significant difference in melting points of the cocrystal and its constituents, it was clear that the isolated crystals were of high purity. Subsequently, both **2-BPXG** and **2-BPXG·4THP** were characterized by FT-IR spectroscopy, DSC, DTA, TGA, HSM, and X-ray diffraction (SCXRD and PXRD).

Description of Structures

2-BPXG. It crystallizes in the monoclinic space group $P2_1/c$. Its molecular structure with the atom labelling scheme is shown in Fig. 1a. Through an N-H···N hydrogen bonding synthon (d/Å: 2.21, θ/°: 160) where one of the N-H bonds is involved with the pyridine nitrogen of another molecule, a ladder-shaped chain structure is formed (Fig. 2). These 1D chains are further extended to a 2D supramolecular network via the other N-H bond and the C=O group of an adjacent molecule with an N-H···O hydrogen bonding synthon (d/Å: 2.21, θ/°: 136). Its packing diagram shown in Fig. S5 provides further stacking in the 2D supramolecular network. The hydrogen bond parameters are listed in Table 2.

2-BPXG·4THP. It crystallizes in the triclinic space group *P*-1, where each unit cell is composed of one **2-BPXG** molecule and four **THP** molecules. Its molecular structure with the atomic labelling scheme is shown in Fig. 1b while its unit cell is represented in Figure S6. In the co-crystal, hydrogen bonding interactions between **2-BPXG** and **THP** molecules form a ladder-shaped chain structure (Fig. 3a), where the amide-pseudo amide motif is present on each end of **2-BPXG** due to the presence of two primary amide groups. Interestingly, **2-BPXG** involves only the primary amide groups in such interactions

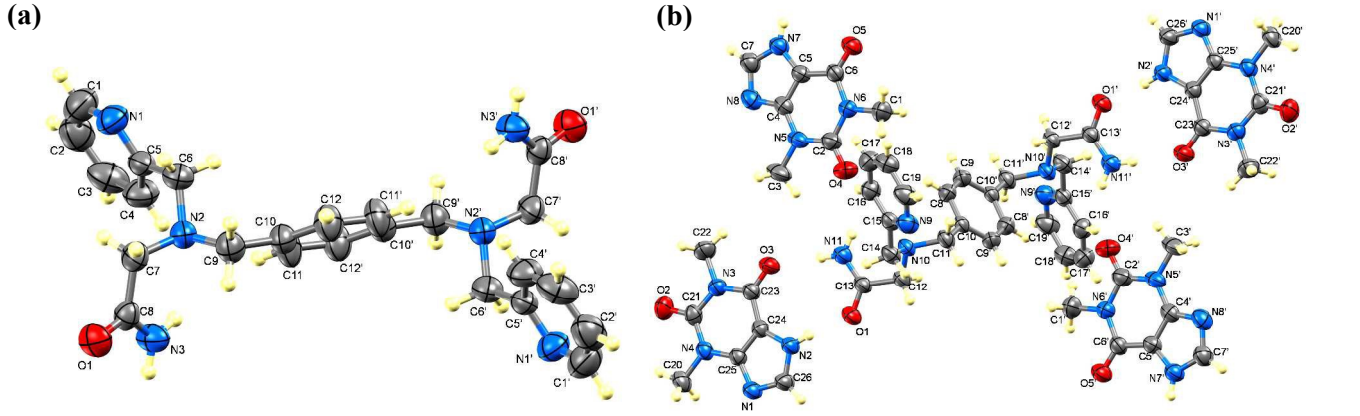

Fig. 1 Molecular structures of (a) **2-BPXG** and (b) **2-BPXG·4THP** with the atomic labelling scheme. Non-hydrogen atoms are depicted as ellipsoids with 50% probability. Hydrogen atoms are represented by spheres with random radius.

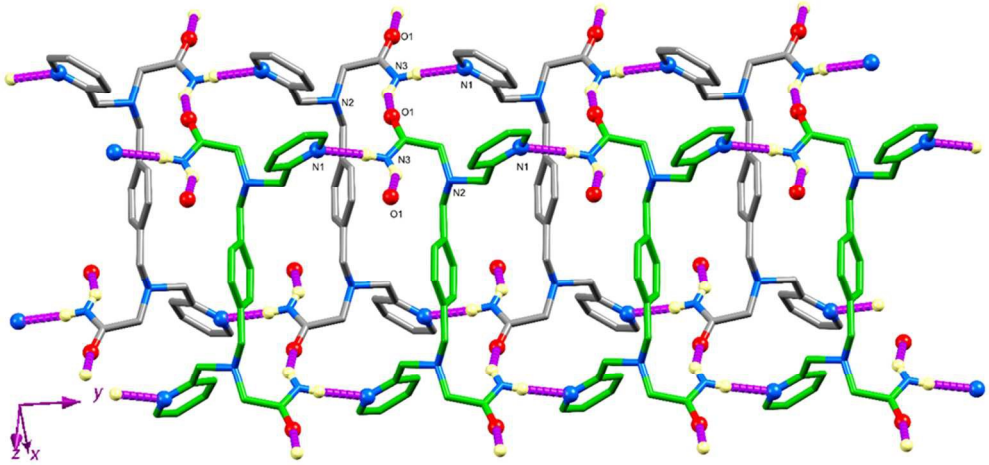

Fig. 2 Schematic representation of the 2D supramolecular network of the ladder-shaped supramolecular assembly via strong hydrogen bonding interactions in **2-BPXG**; hydrogens of carbon atoms are hidden to improve clarity. Symmetry operations to generate equivalent atoms: -x, -y+1, -z+1.

View Article Online
DOI: 10.1039/C7CE01666B

Journal Name RSCPublishing

ARTICLE

leaving the pyridine nitrogens intact. One of the N-H···O hydrogen bonding synthons (d/Å: 1.88, θ/°: 175) is between the

C=O group of **2-BPXG** and the imidazole N-H of **THP**. On the other hand, other N-H···O hydrogen bonding synthons are due to interactions of the NH_2 group with two **THP** molecules via their *endo*-carbonyl O and the *exo*-carbonyl O, respectively. Two of the **THP** molecules form a dimer through the catemeric N-H···N hydrogen bonding (d/Å: 2.07, θ/°: 171), which is uncommon in other **THP** cocrystals; this catemeric N-H···N hydrogen bond is assisted by the weak C-H···O hydrogen bond (d/Å: 2.52, θ/°: 140) involving the imidazole =CH. A similar type of chain connecting the imidazole part of **THP** can be seen in its Form-II.[17] Thus, the intermolecular hydrogen bonds between the amide and each **THP** fulfill the 'best-donor–best-acceptor' rule. The hydrogen bond parameters are listed in Table 2. To the best our knowledge, this is the first example where a coformer with two amide groups has been used to form the amide-pseudo amide hydrogen bonding motif. From this observation, it can be concluded that the amide-pseudo amide motif is a highly favourable interaction. Additionally, strong π-π interactions (centroid to centroid distance: 3.68 Å) and weak C-H···O interactions between the **THP** molecules as shown in Fig. 3b generates an overall 3D supramolecular network in the cocrystal.

(a)

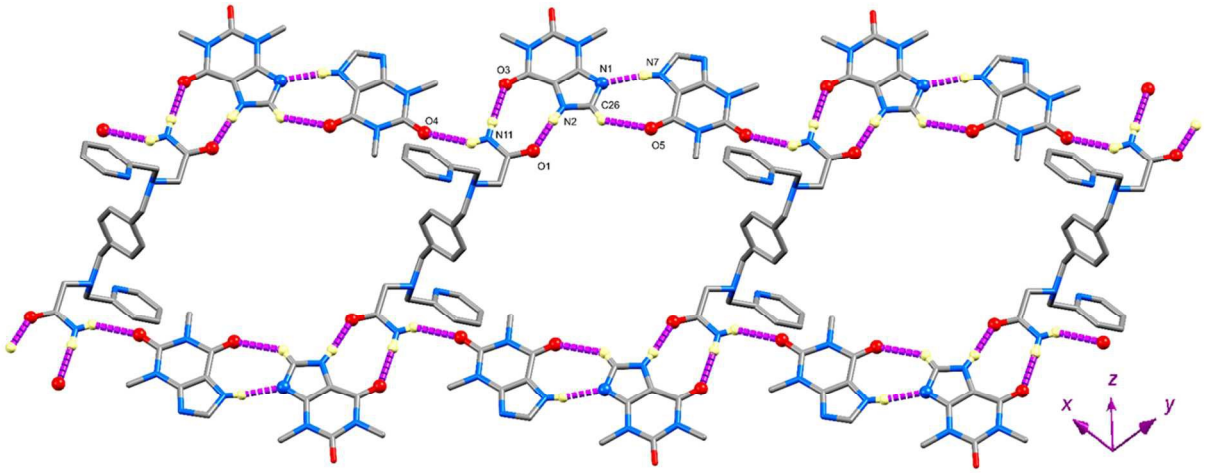

Journal Name
View Article Online
DOI: 10.1039/C7CE01666B
ARTICLE

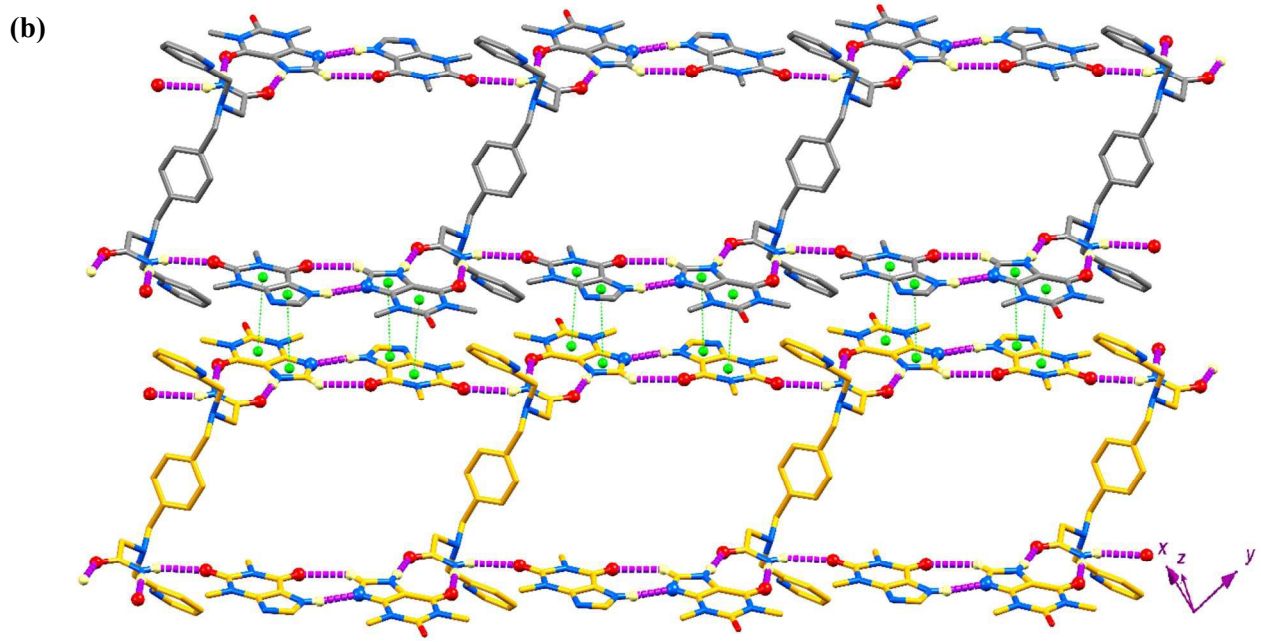

Fig. 3 Schematic representations of (a) a ladder-shaped supramolecular assembly *via* strong hydrogen bonding interactions (color: violet) and (b) 3D supramolecular assembly generated through further connectivity of the ladder-shaped assemblies via strong π-π interactions and weak C-H···O interactions (hydrogens of carbon atoms in **2-BPXG** are hidden for clarity) between the **THP** molecules in **2-BPXG·4THP**. Symmetry operations to generate equivalent atoms: -x+1, -y, -z.

On considering a wider set of **THP**:amide cocrystals published in the CSD and the present work, it is evident that the amide-pseudo amide motif is seen most with all the primary amides[24,27] and secondary amides which are locked in a cis conformation due to being part of a ring (saccharin and 5-fluorouracil).[25-26] For other secondary amide coformers (N-methylformamide and paracetamol),[27,34] where cocrystals with **THP** do not form the amide-pseudo amide motif, it appears that adopting its trans conformation is more energetically favourable than forming this motif.

Table 2 Hydrogen bonding parameters for **2-BPXG** and **2-BPXG·4THP** with symmetry codes[a]

2-BPXG

D–H···A	r (D-H) (Å)	r (H···A) (Å)	r (D···A) (Å)	∠D-H···A (deg)	Symmetry
N(3) —H(3A)···N(1)	0.86	2.21	3.033(6)	160	x,1+y,z
N(3) —H(3B)···N(2)	0.86	2.39	2.768(2)	107	Intramolecular
N(3) —H(3B)···O(1)	0.86	2.21	2.894(2)	136	x,3/2-y,-1/2+z
C(4) —H(4)···O(1)	0.93	2.59	3.500(2)	165	x,3/2-y,-1/2+z
C(11) —H(11)···O(1)	0.93	2.55	3.426(3)	158	x,3/2-y,-1/2+z

2-BPXG·4THP

D–H···A	r (D-H) (Å)	r (H···A) (Å)	r (D···A) (Å)	∠D-H···A (deg)	Symmetry
N(2) —H(2)···O(1)	0.86	1.88	2.732(5)	175	x,y,1+z
N(7) —H(7A)···N(1)	0.86	2.07	2.922(6)	171	x,-1+y,z
N(11) —H(11C)···O(3)	0.86	2.23	3.081(6)	171	x,y,1+z
N(11) —H(11D)···O(4)	0.86	2.42	3.167(6)	145	1+x,y,1+z
N(11) —H(11D)···N(10)	0.86	2.54	2.869(5)	104	Intramolecular
C(26) —H(26)···O(5)	0.93	2.52	3.292(6)	140	x,1+y,z

[a]Numbers in parenthesis are estimated standard deviations in the last significant digits, D = donor, A = acceptor.

View Article Online
DOI: 10.1039/C7CE01666B

Journal Name RSCPublishing

ARTICLE

Hydrogen bond propensities

In order to support the formation of amide-pseudo amide interactions in **2-BPXG·4THP**, hydrogen bond propensity calculations were performed. These calculations take into account which functional groups are involved in hydrogen bonding interactions in the crystal structures of similar molecules present in the CSD and are generated using the Solid Form module in the Mercury v3.5.1 software package.[32] For example, the hydrogen bond donor and acceptor groups of **THP** (T1 and T2) and **2-BPXG** (A) are labelled in Fig. 4, and the resulting propensity values for these are listed in Table 3. The hydrogen bond propensity for a donor–acceptor pair can take a value between 0 and 1, where 0 indicates no likelihood of hydrogen bond formation and a higher value close to 1 indicates a greater likelihood of this bond formation.

For the precursors of the cocrystal, **THP** and **2-BPXG**, the hydrogen bond calculated to have the highest likelihood of formation is that between the NH_2 and C=O moieties of **2-BPXG** (groups labeled d1 and a1 in Fig. 4). Taken into consideration, this result would suggest that **2-BPXG** molecules are more likely to interact with each other, rather than with **THP** molecules, making co-crystallization between **THP** and **2-BPXG** unlikely. When hydrogen bonding propensities relating to the N-H donor group of **THP** (d1) are taken into consideration, however, it is evident that there is a much greater likelihood of this group interacting with the amide oxygen of **2-BPXG** (a1) than with an acceptor group from another theophylline molecule (a3). In fact, the interactions that comprise an amide-pseudo amide interaction between **THP** (d1 - a1) with **2-BPXG** (a1 - d1), respectively, are significantly more likely to occur than any of the possible **THP**−**THP** interactions. This indicates that there is a competition as to whether it is the hydrogen bond donor group of **2-BPXG** (d1) or of **THP** (d1) that will interact with its preferred acceptor.

Hirshfeld surface analysis

The intermolecular interactions present in the solid state of **2-BPXG** and **2-BPXG·4THP** are quantified using Hirshfeld surfaces analysis[35] (HSs) and 2D fingerprint plots[36,37] (FPs). It has allowed visualization of the proportion and nature of the interactions present in the structures, some of which are not readily apparent through examination of the crystal structure alone. These were generated using *Crystal Explorer 3.1*[38] based on the results of single crystal X-ray diffraction studies. Bond lengths to hydrogen atoms were set to standard values. The function d_{norm} is a ratio encompassing the distances of any surface point to the nearest interior (d_i) and exterior (d_e) atom and the van der Waals radii of the atoms:[39]

$$d_{norm} = \frac{(d_i - r_i^{vdW})}{r_i^{vdW}} + \frac{(d_e - r_e^{vdW})}{r_e^{vdW}}$$

Where, r_i^{vdW} and r_e^{vdW} are the van der Waals radii of the atoms. The value of d_{norm} can be negative or positive depending on intermolecular contacts. The negative value of d_{norm} indicates the sum of di and de is shorter than the sum of the relevant van der Waals radii, which is considered to be a closest contact and is visualized as red colour in the HSs. The white colour denotes intermolecular distances close to van der Waals contacts with d_{norm} equal to zero whereas contacts longer than the sum of van der Waals radii with positive d_{norm} values are coloured with blue.

A plot of d_i versus d_e is a 2D fingerprint plot which recognizes the existence of different types of intermolecular interactions. Two additional coloured properties (shape index and curvedness) based on the local curvature of the surface can also be specified. The Hirshfeld surfaces are mapped with d_{norm}, shape index, curvedness and 2D fingerprint plots (full and resolved) presented in this paper.

Table 3 Calculated propensities for hydrogen bond formation between donor and acceptor groups of **THP** and **2-BPXG**[a]

Donor	Acceptor	Propensity
d1 **(A)**	a1 **(A)**	0.96
d1 **(A)**	a2 **(T2)**	0.95
d1 **(A)**	a1 **(T1)**	0.95
d1 **(T1)**	a1 **(A)**	0.92
d1 **(T2)**	a3 **(T1)**	0.73
d1 **(T1)**	a3 **(T2)**	0.73
d1 **(T1)**	a1 **(T2)**	0.88
d1 **(T1)**	a2 **(T2)**	0.88
d1 **(T2)**	a1 **(T2)**	0.88
d1 **(T2)**	a1 **(T1)**	0.88

[a]The labeling of donor and acceptor groups is as shown in **Fig. 4** (T1 & T2 = **THP** groups, A = **2-BPXG** group). Propensities are quoted on a scale from 0 to 1, with higher values indicating a greater likelihood of formation.

The HSs for **2-BPXG** and **2-BPXG·4THP** are illustrated in Fig. 5-7 showing surfaces that have been mapped over a d_{norm} range of -0.18 to 1.4 Å, shape index (-1.0 to 1.0 Å) and curvedness (-4.0 to 0.4 Å), respectively. The surfaces are shown as transparent to allow visualization of all the atoms of the molecule around which they are calculated. The HSs mapped

Journal Name
View Article Online
DOI: 10.1039/C7CE01666B ARTICLE

with d_{norm} showing several red spots suggesting close contacts, the large circular depressions (deep red) visible on the front view and the back view of **2-BPXG**, the surfaces are indicative of hydrogen bonding.[40] Similarly, in **2-BPXG·4THP** the d_{norm} plot showing a deep red spot indicated the presence of an N-H···O hydrogen bonding between **THP** and **2-BPXG** or *vice versa*. The other visible colour spots are observed due to the presence of other close contacts, like H···H, C···H, O···H and N···H.

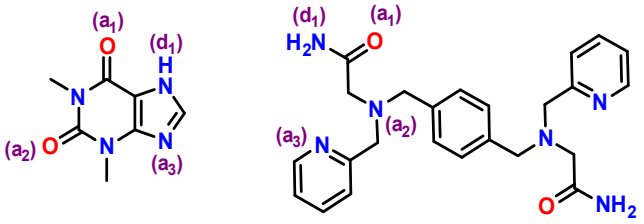

Fig. 4 Hydrogen bond donor and acceptor groups of the molecules **THP** (**T1** and **T2**) and **2-BPXG** (**A**) labelled with reference to the hydrogen bond propensities listed in Table 3.

The shape index is the most sensitive to very subtle changes in surface shape, the red triangles on them (above the plane of the molecule) represent by concave regions indicating atoms of the π-stacked molecule above them, and the blue triangles represent by convex regions indicating the ring atoms of the molecule inside the surfaces.

The curvedness is used to identify the shape of the surface area of the molecule. The flat areas of the surface correspond to low values of curvedness, while sharp curvature areas correspond to high values of curvedness and usually tend to divide the surface into patches, indicating interactions between neighbouring molecules. The large flat region which delineated by a blue outline refer to the π···π stacking interactions. In case of **2-BPXG**, red-yellow colored patches present on flat surface which indicate that there is stacking interaction between the molecules. The molecular electrostatic potential (MEP) is mapped on Hirshfeld

surface using STO-3G basis set at the Hartree-Fock (HF) level ranging from 0.025 a.u. (blue) to −0.025 a.u. (red) (Fig. 8). The molecular electrostatic potential map of **2-BPXG** and **2-BPXG** in **2-BPXG·4THP** revealed that the positive electrostatic

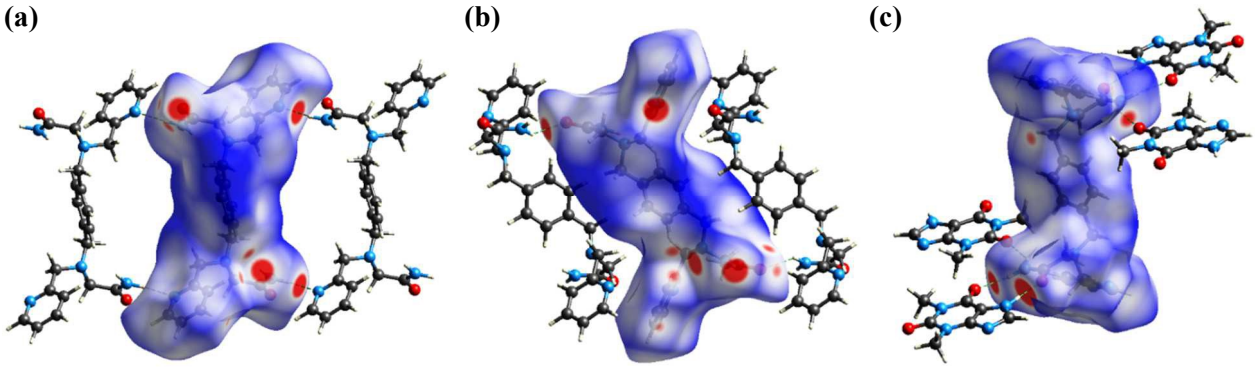

Fig. 5 Hirshfeld surfaces mapped with d_{norm} of (a) front view of **2-BPXG**, (b) back view of **2-BPXG** and (c) front view of **2-BPXG·4THP**.

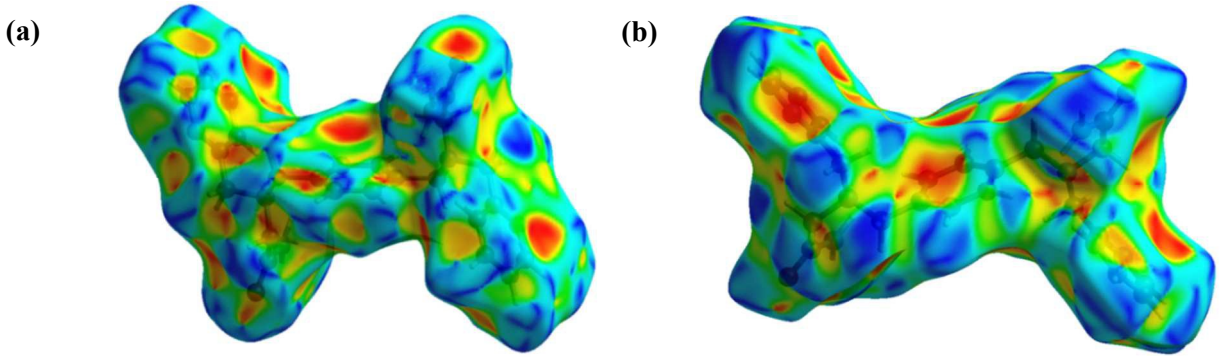

Fig. 6 Hirshfeld surfaces mapped over shape index range from -1.0 to 1.0 Å for (a) **2-BPXG** and (b) **2-BPXG** in **2-BPXG·4THP**.

View Article Online
DOI: 10.1039/C7CE01666B Journal Name

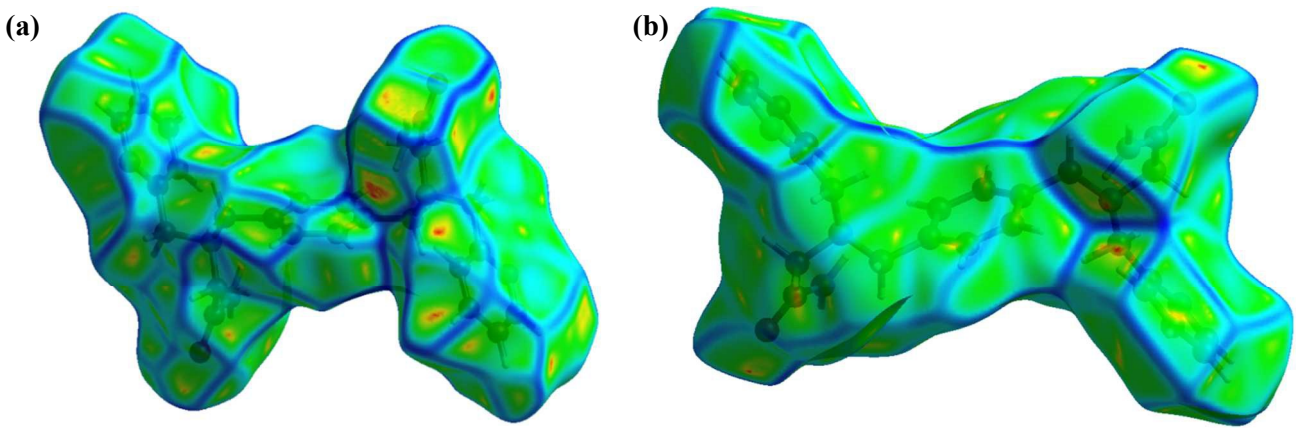

Fig. 7 Hirshfeld surfaces mapped over curvedness range from -4.0 to 0.4 Å for (a) **2-BPXG** and (b) **2-BPXG** in **2-BPXG·4THP**.

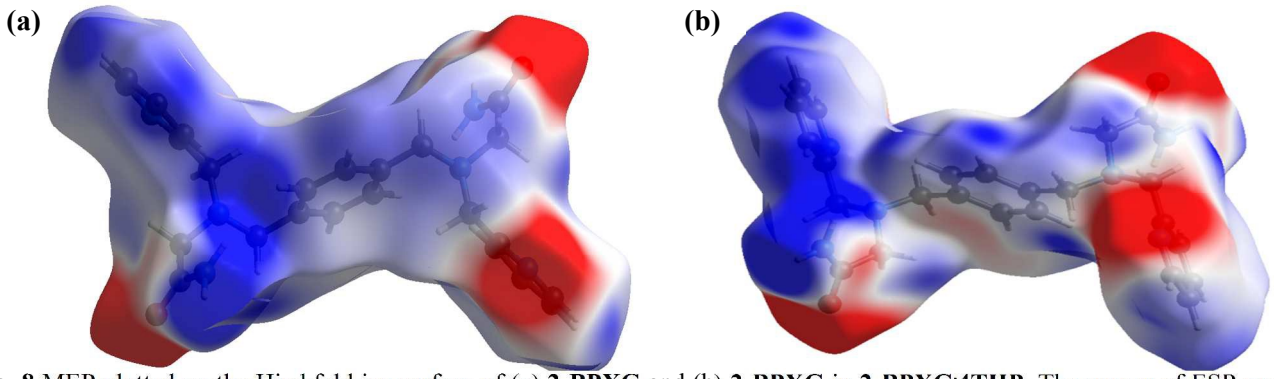

Fig. 8 MEP plotted on the Hirshfeld iso surface of (a) **2-BPXG** and (b) **2-BPXG** in **2-BPXG·4THP**. The ranges of ESP are from 0.025 a. u. (blue) to -0.025 a. u. (red).

potential (blue region) over the surface indicates hydrogen donor potential, whereas the hydrogen bond acceptors are represented by negative electrostatic potential (red region).[41] The crystal geometries were used as input to the *TONTO*[42] integrated with *Crystal Explorer 3.1*.[38]

Quantitative crystal structure analysis

We have further analysed the crystal structure of **2-BPXG** and **2-BPXG·4THP** by looking at the fingerprint plot for different interactions (Fig. 9 and10).[37,43] Fingerprint plot is a unique tool that provides some quantitative information about the individual contribution of the intermolecular interaction in the crystal packing.[44] Some distinct spikes appearing in the 2D fingerprint plot indicate the different interactions motifs in the crystal lattice. Complementary regions are visible in the fingerprint plots where one molecule acts as a donor ($d_e > d_i$) and the other as an acceptor ($d_e < d_i$). In case of **2-BPXG**, the maximum contribution in the fingerprint plot is from H···H contacts (54.7%). This high contribution can be attributed to the presence of NH_2 of the primary amide group, which involves the existence of dispersion interactions as discussed earlier. Four sharp spikes pointing towards lower left of the plot are typical H···O and H···N contacts. For the N···H contacts (10.2%), this contribution is from pyridine nitrogen and amide containing N-H forming the N-H···N interaction. The next contribution is from C···H contacts (18.9%) on account of the presence of C-H···π interactions. The remaining area of the fingerprint plot is occupied by O···H (15.6%) due to N-H···O and C-H···O interactions. Similarly, Hirshfeld surface analyses of **2-BPXG·4THP** show a similar role of H···H interactions (54.5%) compared to its coformer (**2-BPXG**). The

broad region bearing short and narrow spikes at the middle of the plot is reflected as H···H interactions. Two sharp spikes pointing towards lower left of the plot are typical O-H···O hydrogen bonds.

The contribution of H···O contacts (22.0%) is attributed to the N-H···O and C-H···O interactions. The remaining area of the fingerprint plot is occupied by C···H (12.5%) and N···H (8.1%) contact regions. Graphical representation of percentage distribution of different interactions present in **2-BPXG** and **2-BPXG·4THP** as obtained from fingerprint plots are shown in Fig. 11.

View Article Online
DOI: 10.1039/C7CE01666B

Journal Name RSCPublishing

ARTICLE

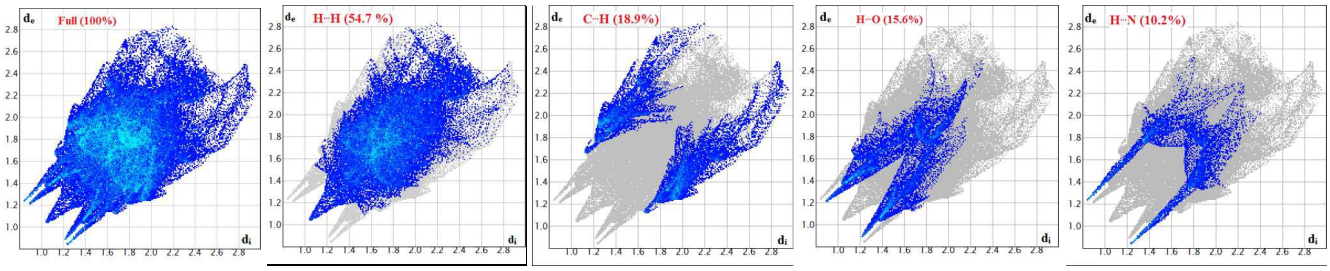

Fig. 9 Two-dimensional fingerprint plots of **2-BPXG** showing the percentage contribution of the individual types of interaction to the total Hirshfeld surface area.

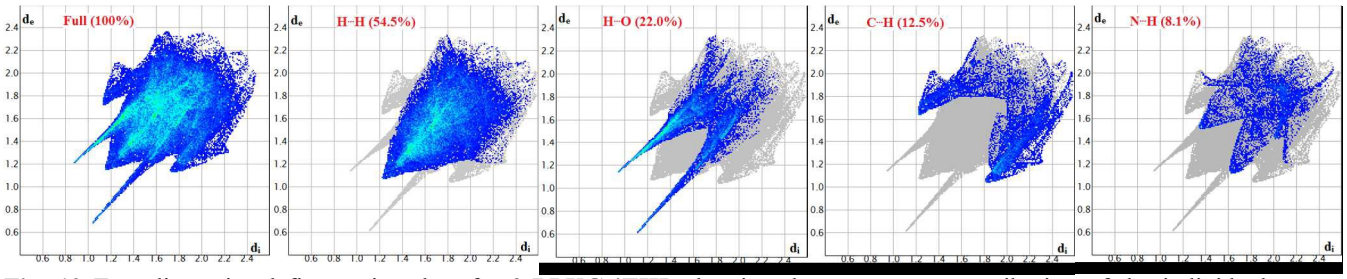

Fig. 10 Two-dimensional fingerprint plots for **2-BPXG·4THP** showing the percentage contribution of the individual types of interaction to the total Hirshfeld surface area.

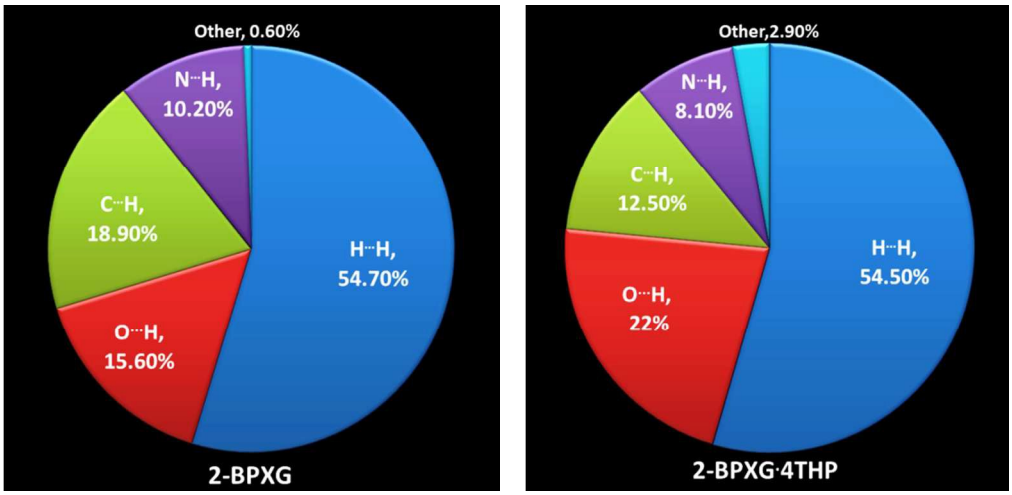

Fig. 11 Graphical representation of percentage distribution of different interactions present in **2-BPXG** and **2-BPXG·4THP** as obtained from fingerprint plots.

FT-IR spectroscopy

FT-IR spectroscopy is a popular analytical method used for studying hydrogen bond formation in cocrystal materials. The spectra of all the compounds were recorded in the solid state as KBr pellets. The asymmetric and symmetric N-H stretching vibrations are observed in the range 3390-3323 cm^{-1} and 3279-3229 cm^{-1}, respectively, due to intermolecular hydrogen bonding. The C-N stretching vibrations of the imidazole ring are observed within the range of 1350-1220 cm^{-1}, however the

View Article Online
DOI: 10.1039/C7CE01666B Journal Name

C-N of the pyrimidine ring absorbs at 1198, 1166, 1147, 1066 cm^{-1} etc. The N-H stretching vibrations appear at a lower region due to extended hydrogen bonding in the cocrystal.[45] The C=O absorption expected for **THP** is at 1718 cm^{-1} and 1668 cm^{-1}, for the primary amide it is expected to appear around 1656 cm^{-1} but these are observed at a lower frequency region i.e. 1704 cm^{-1} and 1648 cm^{-1}, respectively. This changes in frequency is due to participation of the C=O in hydrogen bonding (see Fig. S7).

Thermal analysis

Thermogravimetric analysis (TGA) was used to determine the temperature at which significant mass loss occurs as shown in Fig. 12(a,b,c). Heated at 10 °C min^{-1}, solids of the starting materials **THP** and **2-BPXG** and of the cocrystal remained thermally stable until 210 °C, at which temperature the solids degraded. It clearly shows **2-BPXG·4THP** is less stable (~210 °C) than the individual components **THP** (~230 °C) and **2-BPXG** (~270 °C). In case of 2-BPXG, TGA clearly depicts the phase change (solid to liquid) at 150-160 °C for the melting point, and it starts degradation after 240 °C. On the other hand, both THP and the cocrystal start degradation after the melting point onset.

In order to understand the melting point as a function of temperature, differential thermal analysis (DTA) was carried with a heating rate of 10 °C min^{-1} for all compounds. All DTA thermograms are shown in Fig. 12(d,e,f). **2-BPXG, THP** and **2-BPXG·4THP** exhibited a sharp melting endotherm at 165 °C, 234 °C and 275 °C, respectively. The onset temperature in DTA corresponds to the starting of weight loss in TGA. Thus, the DTA can be used to show that the solid is melting not decomposing, which is further confirmed through HSM.

The DSC traces for the **2-BPXG** and **2-BPXG·4THP** are shown in Fig. S8 and S9, respectively. Both DSC and DTA thermograms show only one major endotherm at 165 °C for **2-BPXG**, which corresponds to its melting temperature, with a melting enthalpy of 128.7 Jg^{-1}, whereas other phase transitions are not observed. In case of **2-BPXG·4THP**, a second endotherm after melting, perhaps due to phase transition or decomposition (*vide infra*, the HSM section). However, its melting point 234 °C and melting enthalpy 85.59 Jg^{-1} are closely comparable. As it is seen, the melting temperature of **2-BPXG·4THP** is higher than that of **2-BPXG** and lower than pure **THP**. The cocrystal formation decreases the melting temperature compared to the pure **THP**. It appears that the intermolecular interactions are responsible for the difference in thermal stability.

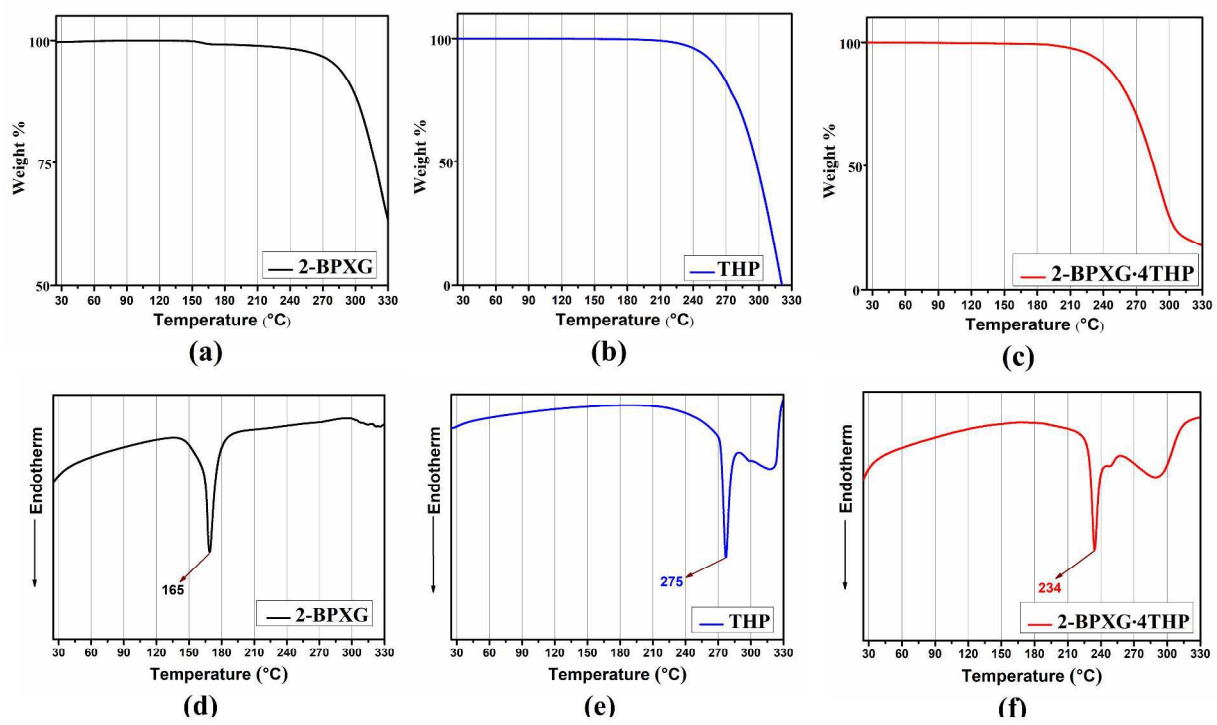

Fig. 12 TGA profiles (a, b and c) and DTA thermograms (d, e and f) of **2-BPXG**, **THP** and **2-BPXG·4THP**, respectively.

Powder X-ray data analysis

To confirm whether the single crystal structure corresponds to the bulk material or not, powder X-ray diffraction patterns were recorded for **2-BPXG**, **THP** and **2-BPXG·4THP** (Fig. 13) at room temperature. The respective experimental and simulated (from the single crystal data) patterns of **2-BPXG** and

View Article Online
DOI: 10.1039/C7CE01666B ARTICLE

2-BPXG·4THP are similar to each other confirming that the single crystal and bulk material properties are the same. It also confirms the phase purity of the bulk sample. Comparing the experimental patterns of **2-BPXG**, **THP** and **2-BPXG·4THP**, it is clearly evident that the cocrystal phase is entirely different from **2-BPXG** and **THP**.

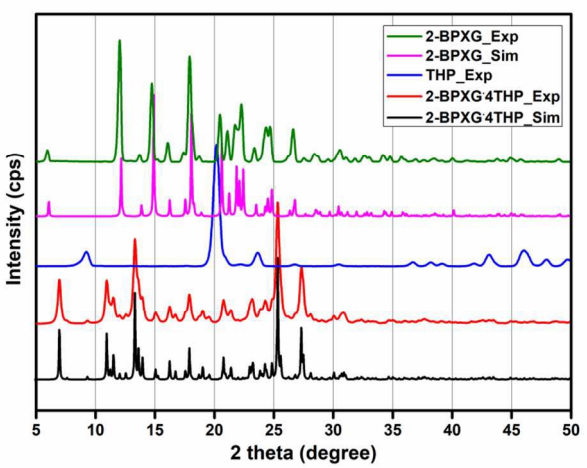

Fig. 13 PXRD patterns of **2-BPXG**, **THP** and **2-BPXG·4THP**.

Hot stage microscopy (HSM)

In order to observe the physical changes during the process of heating, hot stage microscopy (HSM) experiments were performed on crystals of **2-BPXG** and **2-BPXG·4THP** (Fig. 14). As evident from the optical images, the big block crystal of **2-BPXG** and needle shaped crystal of **2-BPXG·4THP** show a prominent change in physical appearance at around 160 °C and 230 °C, respectively. These results support the DSC onset melting temperatures and subsequently become completely melted at 164 °C and 234 °C, respectively (no indication of decomposition).

Concluding Remarks

In summary, we have demonstrated the use of a new coformer **2-BPXG** with two primary amide groups to form a cocrystal with **THP** in a 1:4 ratio, **2-BPXG·4THP**. An overall 2D supramolecular network is formed in **2-BPXG** through the interlinking of the ladder-shaped layers via strong hydrogen bonding between one of the N-H bonds and the carbonyl group of the next molecule. On the other hand, the presence of one primary amide group on each end of the coformer, ladder-shaped layers are formed in the cocrystal via hydrogen bonding between the amide groups (pyridine nitrogens are not involved at all) and the respective complementary functionalities of **THP**. These ladder-shaped layers are then connected to form a 3D supramolecular network *via* strong π-π (centroid to centroid distance: 3.68 Å) and weak C-H···O interactions between the **THP** molecules. With the help of hydrogen bond propensities, Hirshfeld surface analysis and quantitative crystal structure analysis the rare amide-pseudo amide interaction present in **2-BPXG·4THP** was explained in detail. To the best of our knowledge, this is the first example where a coformer with two amide groups has been used to form the amide-pseudo amide hydrogen bonding motif. Thermal properties of **2-BPXG** and **BPXG·4THP** were established from the TGA, DTA, DSC and HSM studies.

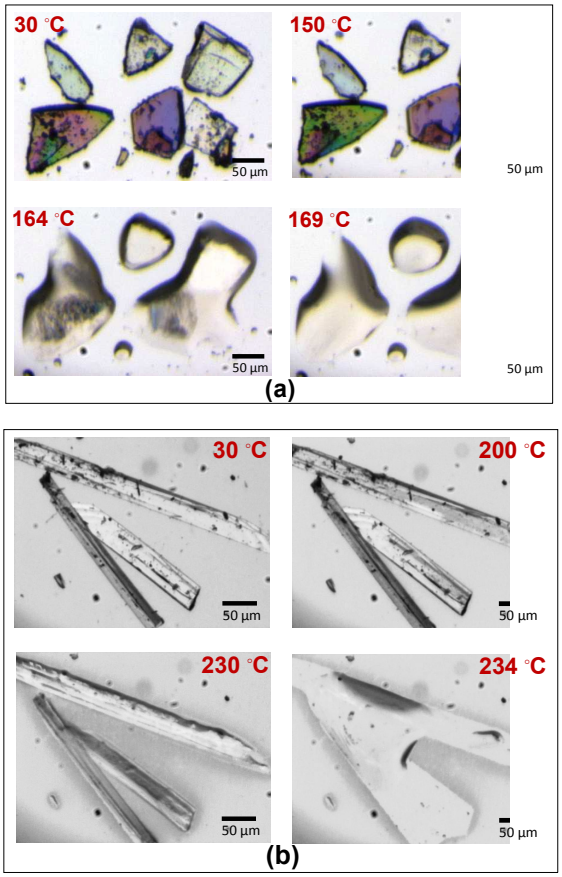

Fig. 14 Hot stage microscopy images of (a) **2-BPXG** and (b) **2-BPXG·4THP** obtained on heating, taken as a function of change in temperature.

Acknowledgements

Funding for this work was provided by IISER, Mohali. D. M. is grateful to the UGC, India, for a research fellowship. The use of X-ray, NMR and SEM central facilities and other departmental facilities at IISER Mohali is acknowledged.

Notes

[a] Department of Chemical Sciences, Indian Institute of Science Education and Research Mohali, Sector 81, Manauli PO, S.A.S. Nagar, Mohali (Punjab) 140306, INDIA
*e-mail: sanjaymandal@iisermohali.ac.in

Electronic Supplementary Information (ESI) available: Crystallographic data of **2-BPXG** and **2-BPXG·4THP** in CIF format (CCDC 1572326 and 1572327, respectively), additional Figures (NMR, DSC, SCXRD and FESEM) for **2-BPXG** and **2-BPXG·4THP**. See DOI: 10.1039/b000000x/

View Article Online
DOI: 10.1039/C7CE01666B Journal Name

References

1 A. V. Trask, W. D. S. Motherwell and W. Jones, *Cryst. Growth Des.*, 2005, **5**, 1013–1021.
2 A. V. Trask, W. D. Motherwell and W. Jones, *Int. J. Pharm.*, 2006, **320**, 114–123.
3 H. D. Clarke, K. K. Arora, H. Bass, P. Kavuru, T. T. Ong, T. Pujari, L. Wojtas and M. J. Zaworotko, *Cryst. Growth Des.*, 2010, **10**, 2152–2167.
4 J. F. Remenar, S. L. Morissette, M. L. Peterson, B. Moulton, J. M. MacPhee, H. R. Guzmán and Ö. Almarsson, *J. Am. Chem. Soc.*, 2003, **125**, 8456–8457.
5 J. I. Wells, *Pharmaceutical Preformulation*, Ellis Horwood, Chichester, 2nd edn., 1993.
6 G. R. Desiraju, *Crystal Engineering: The Design of Organic Solids*, Elsevier, Amsterdam, 1989.
7 W. Jones, in *Organic Molecular Solids*, ed. W. Jones, CRC Press, New York, 1997, pp. 149–199.
8 N. Blagden, M. de Matas, P. T. Gavan and P. York, *Adv. Drug Deliv. Rev.*, 2007, **59**, 617–630.
9 Ö. Almarsson and M. J. Zaworotko, *Chem. Commun. (Camb).*, 2004, 1889–96.
10 M. C. Etter, *J. Phys. Chem.*, 1991, **95**, 4601–4610.
11 D. Stepanovs, M. Jure, L. N. Kuleshova, D. W. M. Hofmann and A. Mishnev, *Cryst. Growth Des.*, 2015, **15**, 3652–3660.
12 T. Grecu, R. Prohens, J. F. McCabe, E. J. Carrington, J. S. Wright, L. Brammerd and C. A. Hunter, *CrystEngComm*, 2017, **19**, 3592–3599.
13 A. Delori, P. T. A. Galek, E. Pidcock, M. Patni and W. Jones, *CrystEngComm*, 2013, **15**, 2916–2928.
14 A. Delori, E. Suresh and V. R. Pedireddi, *CrystEngComm*, 2013, **15**, 4811–4815.
15 M. C. Etter, J. C. MacDonald and J. Bernstein, *Acta Crystallogr., Sect. B: Struct. Sci.*, 1990, **46**, 256–262.
16 D. J. Sutor, *Acta Crystallogr.*, 1958, **11**, 83–87.
17 E. Suzuki, K. Shimomura and K. Sekiguchi, *Chem. Pharm. Bull.*, 1989, **37**, 493–497.
18 L. Seton, D. Khamar, I. J. Bradshaw and G. A. Hutcheon, *Cryst. Growth Des.*, 2010, **10**, 3879–3886.
19 D. Khamar, I. J. Bradshaw, G. A. Hutcheon and L. Seton, *Cryst. Growth Des.*, 2012, **12**, 109–118.
20 M. D. Eddleston, K. E. Hejczyk, E. G. Bithell, G. M. Day and W. Jones, *Chem. - Eur. J.*, 2013, **19**, 7883–7888.
21 Y. Ebisuzaki, P. D. Boyle and J. A. Smith, *Acta Crystallogr., Sect. C: Cryst. Struct. Commun.*, 1997, **53**, 777–779.
22 K. Matsuo and M. Matsuoka, *Cryst. Growth Des.*, 2007, **7**, 411–415.
23 S. Zhang and A. Fischer, *Acta Crystallogr., Sect. E: Struct. Rep. Online*, 2011, **67**, o3357–o3357.
24 B. Legendre and S. Randzio, *Int. J. Pharm.*, 2007, **343**, 41–47.
25 A. V. Trask, W. D. Samuel Motherwell and W. Jones, *Cryst. Growth Des.*, 2005, **5**, 1013-1021.
26 (a) H. Wiedenfeld and F. Knoch, *Arch. Pharm.*, 1986, **319**, 654–659. (b) S. Zaitu, Y. Miwa and T. Taga, *Acta Crystallogr., Sect. C: Cryst. Struct. Commun.*, 1995, **51**, 1857–1859.
27 E. Lu, N. Rodríguez-Hornedo and R. Suryanarayanan, *CrystEngComm*, 2008, **10**, 665.
28 M. D. Eddleston, M. Arhangelskis, L. Fábián, G. J. Tizzard, S. J. Coles and W. Jones, *Cryst. Growth Des.*, 2016, **16**, 51–58.
29 S. Khullar and S. K. Mandal, *Cryst. Growth Des.*, 2012, **12**, 5329–5337.
30 *APEX2, SADABS and SAINT*, Bruker AXS Inc, Madison, WI, USA, 2008.
31 G. M. Sheldrick, *Acta Crystallogr., Sect. A: Found. Crystallogr.*, 2008, **64**, 112–122.
32 C. F. Macrae, I. J. Bruno, J. A. Chisholm, P. R. Edgington, P. McCabe, E. Pidcock, L. Rodriguez-Monge, R. Taylor, J. van de Streek and P. A. Wood, *J. Appl. Crystallogr.*, 2008, **41**, 466–470.
33 A. L. Spek, *PLATON, Version 1.62*, University of Utrecht, 1999.
34 H. L. Lee and T. Lee, *CrystEngComm*, 2015, **17**, 9002–9006.
35 M. A. Spackman and D. Jayatilaka, *CrystEngComm*, 2009, **11**, 19–32.
36 M. A. Spackman and J. J. McKinnon, *CrystEngComm*, 2002, **4**, 378–392.
37 J. J. McKinnon, D. Jayatilaka and M. A. Spackman, *Chem. Commun.*, 2007, 3814–3816.
38 S. K. Wolff, D. J. Grimwood, J. J. McKinnon, M. J. Turner, D. Jayatilaka and M. A. Spackman, *CrystalExplorer 3.1*, University of Western Australia, 2012.
39 F. L. Hirshfeld, *Theor. Chim. Acta*, 1977, **44**, 129–138.
40 S. K. Seth, D. Sarkar, A. Roy and T. Kar, *CrystEngComm*, 2011, **13**, 6728–6741.
41 P. A. Wood, J. J. McKinnon, S. Parsons, E. Pidcock and M. A. Spackman, *CrystEngComm*, 2008, **10**, 368–376.
42 D. Jayatilaka, D. J. Grimwood, A. Lee, A. Lemay, A. J. Russel, C. Taylor, S. K. Wolff, P. Cassam-Chenai and A. Whitton, *TONTO*, Available at: http://Hirshfieldsurface.net/2005.
43 A. Parkin, G. Barr, W. Dong, C. J. Gilmore, D. Jayatilaka, J. J. McKinnon, M. A. Spackman and C. C. Wilson, *CrystEngComm*, 2007, **9**, 648–652.
44 M. A. Spackman and P. G. Byrom, *Chem. Phys. Lett.*, 1997, **267**, 215–220.
45 B. Sarma and B. Saikia, *CrystEngComm*, 2014, **16**, 4753–4765.

View Article Online
DOI: 10.1039/C7CE01666B

Journal Name

RSCPublishing

ARTICLE

Table of Contents artwork

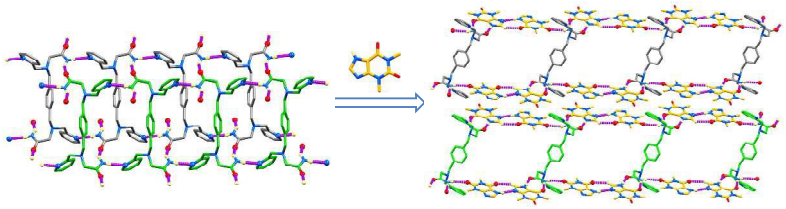

Double the FUN! A rare amide-pseudo amide hydrogen bonding motif has been established for the co-crystal between theophylline and a new coformer with two primary amide groups.